



# OPEN Controlling Mie scattering response to refractive index variations via light field manipulation

Jianzhi Zeng<sup>1</sup>, Hanqing Cai<sup>1</sup>, Jiachen Liu<sup>1,2,3</sup> & Haifeng Hu<sup>1,2,3</sup>✉

We present an efficient method for determining the T-matrix of axisymmetric particles using the finite element method (FEM) in conjunction with an analytical approach that expands the scattered field using vector spherical harmonics (VSHs). To tailor the response of nanoparticles under complex optical field excitation, we design the incident field based on the T-matrix, which comprehensively describes the relationship between the incident and scattered fields. The sensitivity of scattering field to environmental refractive index can be effectively controlled by introducing the concepts of principal modes (PMs) and anti-principal modes (anti-PMs), which used to be utilized to control frequency dispersion of multi-channel light scattering. Our approach diverges from previous research by emphasizing the manipulation of refractive index sensitivity in Mie particles, rather than focusing on controlling scattering response in the frequency domain. Additionally, we employ an inverse design method to determine the light field distribution on the entrance pupil plane, which can be used to generate the designed PMs and anti-PMs after tightly focusing by high-NA objective. This work presents new degrees of freedom for controlling light-matter interactions in modern optics. It is expected to find wide-ranging applications in the fields of optical sensing and measurement.

**Keywords** T-matrix, Light field manipulation, Principal modes, Anti-principal modes, Tightly focused field

The T-matrix method, originally introduced by Peter C. Waterman in the 1960s, is a powerful numerical technique for solving light scattering problems<sup>1</sup>, particularly suitable for addressing scattering problems involving non-spherical and complex-shaped particles. The T-matrix method solves the scattering problem by establishing relationships between the incident field, scattered field, and internal field through boundary conditions, significantly enhancing computational efficiency and applicability<sup>2</sup>. The extended boundary condition method (EBCM) is commonly used for analytical T-matrix calculations. However, it requires high numerical accuracy and is prone to non-convergence. Additionally, calculating the T-matrix through numerical methods involves complex three-dimensional scattering computations, which demand substantial computational resources and processing time. Today, the T-matrix method can be used to study the scattering and absorption characteristics of aerosol particles in the atmosphere<sup>3</sup>, aiding in a better understanding and prediction of climate change; it can be applied in optical coherence tomography and other imaging techniques to simulate light scattering by cells and other microstructures in biological tissues<sup>4</sup>; and it can investigate the light scattering properties of material surfaces to develop materials with specific optical characteristics<sup>5</sup>.

In the study of light-particle interactions, early research primarily focused on optimizing scattering effects by adjusting parameters such as the geometry, size, and material properties of the particles. For instance, the shape design of nanoparticles (e.g., nano-disk) can effectively enhance the excitation of anapole modes, generating non-radiative modes<sup>6</sup>. However, this approach often relies on fixed particle parameters, making dynamic control of the scattered light field challenging. In recent years, research has gradually shifted towards the manipulation of the incident light field itself. For example, by controlling the polarization, phase, and amplitude of the incident light field, it is possible to enhance the excitation of specific modes, such as the anapole mode, under fixed particle structures<sup>7</sup>. This can enhance circular dichroism signal measurements of chirality without changing the particles themselves<sup>8</sup>, thereby effectively controlling the interaction between light and matter to achieve specific optical responses. At the same time, light field manipulation techniques have been used to improve the resolution of microscopes, breaking the diffraction limit of conventional optical microscopy<sup>9</sup>. Light field manipulation techniques can be also utilized to capture and manipulate tiny particles or biomolecules<sup>10</sup>.

<sup>1</sup>School of Optical-Electrical and Computer Engineering, University of Shanghai for Science and Technology, Shanghai 200093, China. <sup>2</sup>Zhangjiang Laboratory, 100 Haik Road, Shanghai 201204, China. <sup>3</sup>Shanghai Key Laboratory of Modern Optical System, University of Shanghai for Science and Technology, Shanghai 200093, China. ✉email: hfh@usst.edu.cn

Dynamic control is also of significant importance in sensing and measurement, enabling real-time monitoring of environmental parameters such as temperature, pressure, and gas concentration<sup>11</sup>. Moreover, dynamic light field manipulation is used to enhance the resolution and sensitivity of biomedical imaging, allowing for real-time monitoring of biological processes<sup>12</sup>. In quantum metrology, dynamic light field manipulation is employed to improve measurement precision and reduce noise interference<sup>13</sup>. In the field of refractive index sensing research, responses sensitive to refractive index can be achieved by manipulating the physical and chemical properties of sensing particles<sup>14</sup>. Furthermore, specific optical responses can be achieved by modulating the frequency domain characteristics of the fiber transmission matrix. The principal modes (PMs) and the anti-principal modes (anti-PMs)<sup>15</sup> are the means of such regulation. This theory originates from the field of quantum scattering, particularly from studies on the time dynamics of wave scattering in complex systems, encompassing quantum mechanics, nuclear physics, acoustics, and optics<sup>16</sup>. Most research has focused on the statistics of delay times, specifically the eigenvalues of the Wigner-Smith time delay matrix<sup>17</sup>. Subsequently, the Wigner-Smith eigenstates<sup>18</sup> were introduced into multimode fibers (MMF) as a generalization of the polarization principal states in single-mode fibers, referred to as PMs in MMF to suppress modal dispersion<sup>16</sup>. Tight focusing systems are commonly used to manipulate optical fields, which has many advantages in characterizing light fields, allowing light to be focused into a very small volume, thus achieving high spatial resolution<sup>19</sup>. It also enables precise control over the phase, amplitude, and polarization of the light field, facilitating complex light field manipulation and control<sup>20</sup>. Additionally, tight focusing can effectively reduce background noise, improving the quality and reliability of the signal<sup>21</sup>. The interaction between particles and tightly focused light fields is highly significant, such as conventional optical tweezers and near-field optical trapping, which are highly popular in bio-sciences<sup>22,23</sup>. However, studies on designing light fields from this interaction<sup>24</sup> are relatively scarce. Since tightly focused light fields can be expanded using vector spherical harmonics, the T-matrix method serves as a powerful and effective tool for this research. Moreover, the introduction of the concept of PMs within the T-matrix framework is both practical and efficient. This innovation opens up a new dimension in light field manipulation.

In this work, we proposed an optical field manipulation method, which can modify the response of scattered field by nanoparticle to the environmental refractive index. The main contribution of this work is to introduce the concepts of PMs and anti-PMs during Mie scattering processes. As discussed above, T-matrix is a powerful tool to analyze the scattering effect of Mie particle. Our study combines the finite element method (FEM) and vector spherical harmonics (VSHs) expansion to calculate the scattering coefficients, providing an efficient and accurate approach for determining the T-matrix of particles. Subsequently, in the study of light-matter interactions, we have moved beyond the conventional approach of modifying particle properties to affect optical responses. Instead, we focus on dynamically controlling these responses by manipulating the high-degree-of-freedom characteristics of the incident light field. Our study builds upon the theoretical framework of the Wigner-Smith time delay matrix, traditionally used to describe time delay relationships between different scattering channels in multi-channel systems. We extend this concept by modifying the matrix to account for changes in the refractive index of the medium, thus enabling the control of refractive index sensitivity, which is a novel degree of freedom in describing light-matter interactions. Through the analysis of eigenvectors of the matrix, we identify a light field (PMs) that is insensitive to refractive index changes, thereby suppressing the influence of refractive index changes in the medium on particle scattering effects. Simultaneously, by making a series of alterations and optimizations to the aforementioned matrix, we can further identify anti-PMs that is sensitive to refractive index changes, used to enhance the impact of refractive index variations on particle scattering effects. Ultimately, we propose a method to apply the PMs and anti-PMs fields upon Mie particles, which is implemented utilizing a tightly focused system. To perform inverse design of the incident paraxial beam, we establish the M-matrix of the tightly focused system to describe its optical properties, enabling the realization of these two modes within specific optical systems. This work marks a substantial advancement in the dynamic manipulation of light fields, holding great potential for applications in sensing, imaging, measurement, and other advanced technologies.

## Results and methods

### T-matrix of particles

In this section, we primarily discuss the calculation method for the T-matrix of axisymmetric particles. According to Lorenz-Mie theory, the expressions for the incident field and the scattered field are as follows<sup>25</sup>:

$$\mathbf{E}_{inc}(r, \theta, \phi) = \sum_{\nu=1}^{\nu_{\max}} \sum_{\mu=-\nu}^{\nu} [a_{\mu\nu} Rg\mathbf{M}_{\mu\nu}(k_0 r, \theta, \phi) + b_{\mu\nu} Rg\mathbf{N}_{\mu\nu}(k_0 r, \theta, \phi)], \quad (1)$$

$$\mathbf{E}_{sca}(r, \theta, \phi) = \sum_{\nu=1}^{\nu_{\max}} \sum_{\mu=-\nu}^{\nu} [p_{\mu\nu} \mathbf{M}_{\mu\nu}(k_0 r, \theta, \phi) + q_{\mu\nu} \mathbf{N}_{\mu\nu}(k_0 r, \theta, \phi)], \quad (2)$$

where  $k_0$  is the wave number in the surrounding medium,  $a_{\mu\nu}$  and  $b_{\mu\nu}$  are the coefficients of the incident field,  $p_{\mu\nu}$  and  $q_{\mu\nu}$  are the coefficients of the scattered field. The VSH functions  $Rg\mathbf{M}$  and  $Rg\mathbf{N}$  are regular (finite) at the origin, while the VSH functions  $\mathbf{M}$  and  $\mathbf{N}$  which include a singularity respectively, are infinite at the origin. The specific relationship between the T-matrix and the incident and scattered fields is as follows:

$$\begin{bmatrix} p_{\mu\nu} \\ q_{\mu\nu} \end{bmatrix} = \mathbf{T} \begin{bmatrix} a_{\mu\nu} \\ b_{\mu\nu} \end{bmatrix}, \quad (3)$$

the dimension of the T-matrix depends on the values for maximum order of  $\nu$  (i.e.  $\nu_{max}$ ).

For spherical particles, we can use theoretical formulas combined with numerical calculations to obtain the T-matrix. For non-spherical particles, we can use simulations combined with numerical calculations to determine the T-matrix.

Firstly, we define the particle to be analyzed. As shown in Fig. 1(a), we consider a hollow cylinder particle with a high refractive index of  $n_1 = 3$ , which is placed in a medium with  $n_2 = 1.33$ . The inner and outer diameters of the particle are represented by  $R_{in}$  and  $R_{out}$ . The height of the particle is  $L$ . According to the definition of T-matrix, each column of T-matrix representing the expansion coefficients of the scattered field obtained by exciting the particle with a specific VSH as the incident field. Therefore, to determine the T-matrix, the first step is to solve the scattering field under the incidence of each regular VSH field (i.e.  $RgM_{\mu\nu}$  or  $RgN_{\mu\nu}$ ). Then, the second step is to calculate the corresponding expansion coefficients by decomposing the scattering field using orthogonal relation between VSHs. Finally, the T-matrix can be reconstructed by all its columns obtained from the expansion coefficients. During the calculation of T-matrix, a large number of three-dimensional scattering problems need to be solved. For nonspherical Mie particles, these scattering problems are difficult to handle with analytical methods. Enhancing the calculation efficiency of the T-matrix is crucial for advancing the application of this method.

In this work, we use FEM to solve the scattering problem. For the axisymmetric three-dimensional particles as shown in Fig. 1(a), when the incident field possesses an azimuthal angle dependence of  $e^{-i\mu\varphi}$ , the azimuthal order  $\mu$  is conserved in the scattering process, meaning that the scattered field also exhibits the same  $\mu$ -order.

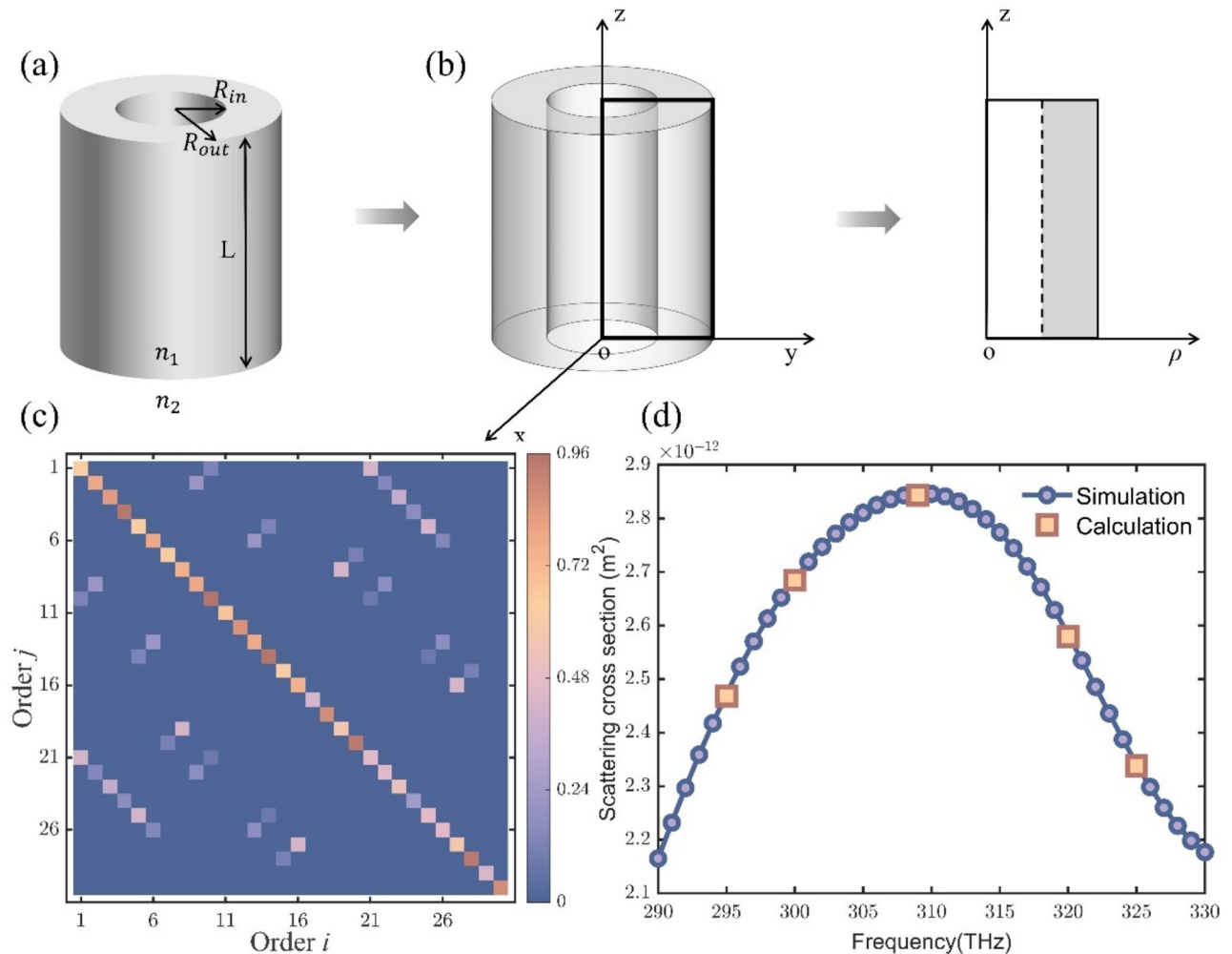


**Fig. 1.** Schematic diagram of the T-matrix calculation method for axisymmetric homogeneous medium particles. (a) Schematic diagram of the hollow cylindrical particle. (b) dimensional reduction: from a three-dimensional axisymmetric model to a two-dimensional model for enhanced computational efficiency. (c) The calculated T-matrix of the particle (only the part with  $\nu = 1, 2, 3$  is shown). (d) Relationship graph between scattering cross-section of the particle and the incident light frequency, verifying the accuracy of the T-matrix.

Within the cylindrical coordinate system  $(\rho, \varphi, z)$ , considering the axisymmetric condition, the electric field  $\mathbf{E}(\rho, \varphi, z)$  should be expressed as  $\mathbf{E}(\rho, z)e^{-i\mu\varphi}$ . Thus, the three-dimensional scattering model can be simplified to a two-dimensional model, which only requires determining the field components that depend on  $\rho$  and  $z$  as shown in Fig. 1(b). To integrate the VSH field as the incident field in the model, the coordinate transformation between spherical and cylindrical coordinates, as outlined in Eq. (4), must be taken into account.

$$\begin{bmatrix} \mathbf{n}_\rho \\ \mathbf{n}_\varphi \\ \mathbf{n}_z \end{bmatrix} = \begin{bmatrix} \sin \theta & \cos \theta & 0 \\ 0 & 0 & 1 \\ \cos \theta & -\sin \theta & 0 \end{bmatrix} \begin{bmatrix} \mathbf{n}_r \\ \mathbf{n}_\theta \\ \mathbf{n}_\phi \end{bmatrix} \quad (4)$$

In this manner, the scattering field of the particle can be simulated, the corresponding scattering coefficients can be calculated, and the T-matrix for the particle can ultimately be obtained. We selected a maximum order of  $\nu_{\max} = 10$  to adequately describe the scattering characteristics of the particle. In Fig. 1(c), we present a portion of the T-matrix only including the VSH order with  $\nu = 1, 2, 3$ . For the VSHs with larger 3, the scattering efficiencies become much lower than the first orders. Each column in the figure corresponds to the scattering coefficients obtained from the incident field of the corresponding vector spherical harmonic with unit amplitude.

Subsequently, we verified the accuracy of the derived T-matrix by calculating the scattering cross-section at different frequencies, as shown in Fig. 1(d). The blue line represents the actual scattering cross-section values obtained from simulations under the illumination of a y-polarized plane wave propagating in the x-direction at a vacuum wavelength of 970 nm, while the yellow squares indicate the scattering cross-section values calculated from the already obtained T-matrix (with  $\nu_{\max} = 10$ ). It is evident that the results closely match the simulation values, thereby validating the accuracy of our approach to solving the T-matrix problem. In the supplementary material, the scattered field is reconstructed using the scattering coefficients derived from T-matrix method. This reconstructed field was then compared to the scattered field generated by the finite element method, providing additional validation for the accuracy of our method of determining the T-matrix of particles.

### Principal modes

In this work, we introduce the Wigner-Smith operator into the T-matrix theory to manipulate the refractive index sensitivities of particles during optical scattering process, which is defined as  $\mathbf{Q}$ <sup>16</sup>. The specific expression is as follows:

$$\mathbf{Q} = -i\mathbf{T}^{-1} \frac{\partial \mathbf{T}}{\partial n}, \quad (5)$$

where  $\mathbf{T}$  represents the previously calculated T-matrix, and  $n$  is the refractive index. The  $\mathbf{Q}$  operator can be derived by T-matrix and the first-order derivative of T-matrix. Then, the eigenvectors of  $\mathbf{Q}$  operator provide the incident field for the PMs. These are the unique input states, and the first-order derivative of the output field with respect to the refractive index vanishes at a specific refractive index. To enhance the interaction between incident light and the particle considered in the work, only VSHs with  $\nu = 1, 2$  and 3 are used to construct the PMs, which can eliminate the influence of high order VSH field<sup>25</sup>. To verify the properties of the PMs, the accurate scattering field is calculated by the full T-matrix with  $\nu_{\max} = 10$ . Furthermore, according to the T-matrix in Fig. 1(c), the  $\mu$ -order VSH fields are decouple from other components with different azimuthal orders (i.e.  $\mu \neq \mu$ )<sup>25</sup>. In our work, the incident light field are only composed of VSHs with  $\mu = 1$ , so the expansion of VSHs of PMs and anti-PMs in Eq. (1) can be simplified as:

$$\mathbf{E}_{inc}(r, \theta, \phi) = \sum_{\nu=1}^3 [a_\nu Rg\mathbf{M}_\nu(k_0r, \theta, \phi) + b_\nu Rg\mathbf{N}_\nu(k_0r, \theta, \phi)] \quad (6)$$

In Eq. (6), the expansion coefficients of  $a_\nu$  and  $b_\nu$  are from the eigen vector of  $\mathbf{Q}$  operator in Eq. (5). In the following discussion, we use these expansion coefficients to represent the incident states, which is denoted by  $\Xi = [a_\nu, b_\nu]^T$ . Meanwhile, the scattering field is denoted by  $\Psi = [p_\nu, q_\nu]^T$  in the similar way. The T-matrix is altered when there is a change in the environmental refractive index, and the scattering field, which is dependent on the index, can be computed using Eq. (7).

$$\Psi(n) = \mathbf{T}(n)\Xi \quad (7)$$

To evaluate the variation of scattering field versus refractive index, the self-correlation function is defined in Eq. (8).

$$C(n, n_0) = \frac{|\Psi(n)\Psi(n_0)|}{|\Psi(n)||\Psi(n_0)|} \in [0, 1] \quad (8)$$

In Eq. (8), the self-correlation function is determined by the normalized scattering coefficient vector, hence its value should fall within the range of [0, 1]. When the function attains its maximum value of one, it signifies that the two vectors of  $\Psi(n)$  and  $\Psi(n_0)$  are identical.

In the simulation model, we use the obtained PMs at a vacuum wavelength of 970 nm to illuminate the particle immersed in a medium with variable refractive index from 1.33 to 1.35 and obtain a set of scattering

field coefficients. After that, we select a y-polarized plane wave propagating in the x-direction and the same frequency to illuminate the same particle immersed in a medium with varying refractive index from 1.33 to 1.35, resulting in another set of scattered field coefficients. The self-correlation functions calculated from the two sets of scattered fields and their correlation function under different refractive index are shown in Fig. 2(a).

It can be clearly seen from Fig. 2(a) that due to the vanishing of the first-order derivative of the PM, the correlation function curve becomes extremely flat. Compared with the plane wave, PMs make its influence of the refractive index on scattered field almost negligible, thereby demonstrating the effectiveness of the aforementioned method.

### Anti-principal modes

Building upon the concept of utilizing PMs to render the scattering field insensitive to refractive index variations, we now propose an approach that achieves the opposite effect, making the scattering field highly sensitive to changes in environmental refractive index. To achieve this goal, the concept of anti-PMs is proposed based on the optimization method. When we use the anti-PM field as the incident field on the particle, the decorrelation of scattering field is maximized as soon as the refractive index deviates from its original value. The determination of these anti-PMs will be facilitated by employing a standard optimization technique in the following part. To carry out the optimization process, we define the loss function as shown in Eq. (9).

$$\Gamma(\Xi) = \int dn [1 - C(n, n_0)^2] W(n) = \int dn [1 - \frac{|\Psi^\dagger(n) \cdot \Psi(n_0)|^2}{|\Psi(n)|^2 |\Psi(n_0)|^2}] W(n) \\ = \int dn [1 - \frac{|\Xi^\dagger T^\dagger(n) T(n_0) \Xi|^2}{|T(n) \Xi|^2 |T(n_0) \Xi|^2}] W(n) \quad (9)$$

In this loss function, the effective range of refractive indices is defined by the weight function  $W(n)$ , which is chosen to be a stepwise continuous function starting from  $n_0 = 1.33$ , as shown in Fig. 2(b). To obtain the refractive index-sensitive anti-PMs, the scalar value of  $\Gamma$  needs to be maximized based on gradient descent algorithm. The derivative of  $\Gamma$  with respect to the incident field can be expressed as Eq. (10).

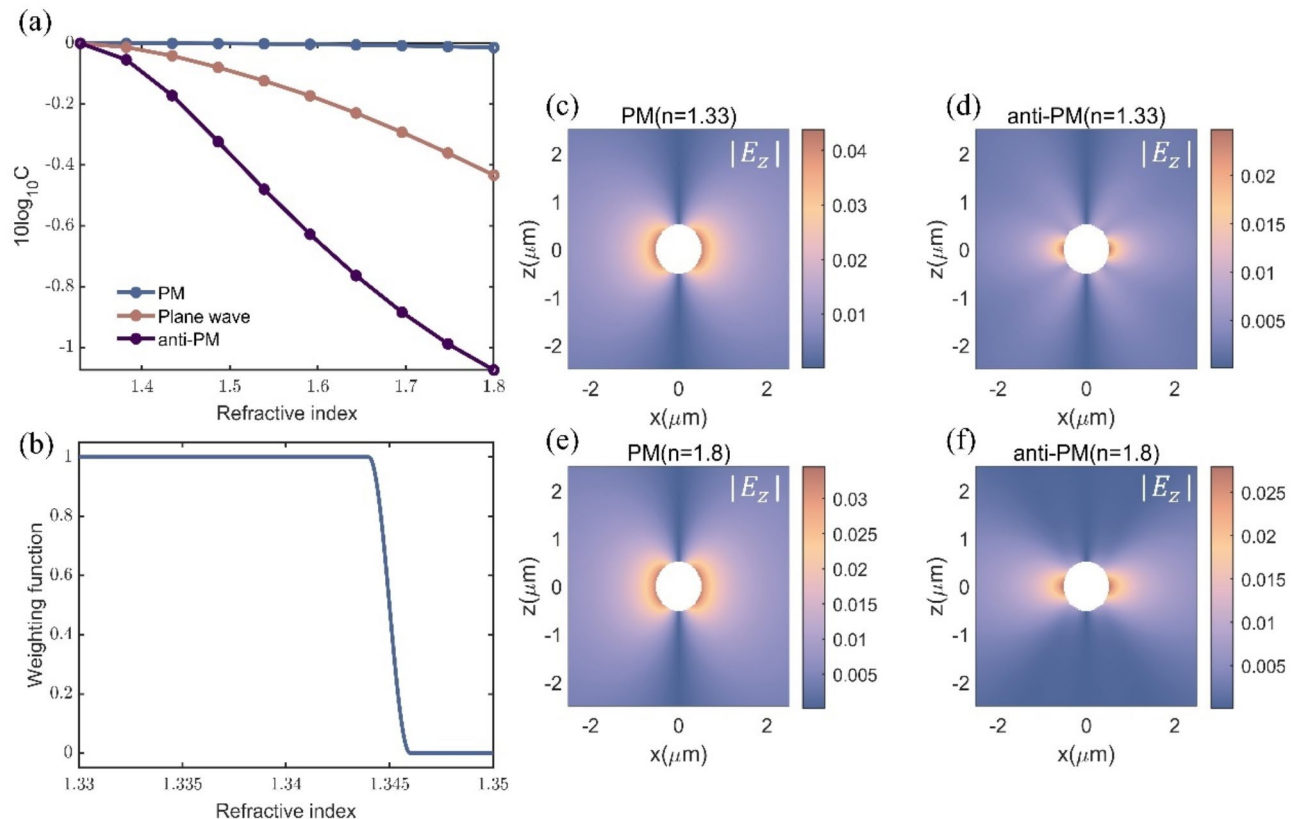


**Fig. 2.** (a) The relationship between the correlation functions and the refractive index of the external medium surrounding the particles under the incidence of PM, anti-PM and plane wave. (b) The wight function in the loss function to optimized the anti-PM field. (c–f) The distributions of the scattered field of particle in environments with different refractive indices (i.e.  $n = 1.33$  and  $n = 1.8$ ) and under various incident light (i.e. PM and anti-PM).



$$\begin{aligned}
\frac{\partial \Gamma}{\partial \Xi^\dagger} = & \int dn [\mathbf{T}^\dagger(n) \mathbf{T}(n_0)] \Xi \frac{-\Xi^\dagger \mathbf{T}^\dagger(n_0) \mathbf{T}(n) \Xi}{|\mathbf{T}(n) \Xi|^2 |\mathbf{T}(n_0) \Xi|^2} \\
& + \mathbf{T}^\dagger(n_0) \mathbf{T}(n) \Xi \frac{-\Xi^\dagger \mathbf{T}^\dagger(n) \mathbf{T}(n_0) \Xi}{|\mathbf{T}(n) \Xi|^2 |\mathbf{T}(n_0) \Xi|^2} \\
& + \mathbf{T}^\dagger(n) \mathbf{T}(n) \Xi \frac{|\Xi^\dagger \mathbf{T}^\dagger(n) \mathbf{T}(n_0) \Xi|^2}{|\mathbf{T}(n) \Xi|^4 |\mathbf{T}(n_0) \Xi|^2} \\
& + \mathbf{T}^\dagger(n_0) \mathbf{T}(n_0) \Xi \frac{|\Xi^\dagger \mathbf{T}^\dagger(n) \mathbf{T}(n_0) \Xi|^2}{|\mathbf{T}(n) \Xi|^2 |\mathbf{T}(n_0) \Xi|^4} W(n)
\end{aligned} \quad (10)$$

The update equation of the optimization algorithm can be represented as follows:

$$\Xi_{t+1} = \frac{1}{N_{t+1}} (\Xi_t - \frac{\partial \Gamma}{\partial \Xi^\dagger} |_{\Xi_t} \Delta s), \quad (11)$$

where  $\Delta s$  is the appropriate step size,  $t$  is the number of iterations, and  $N_{t+1}$  is the normalization constant ensuring  $|\Xi_{t+1}| = 1$ . The initial incident field coefficient  $\Xi$  is iteratively selected from the previously obtained PMs. When the loss function  $\Gamma$  approaches a constant value, we can obtain the anti-PMs that enhances the influence of refractive index variations on scattering. Under the illumination of PMs field, we can obtain a set of scattering field coefficients for the particle immersed in medium of different refractive index. By substituting these coefficients into the correlation function defined in Eq. (9), we can compute the curve shown in Fig. 2(a). One can note that the curve exhibits a more pronounced decline with changes in the refractive index when compared to the case of plane wave incidence. The key to obtaining PMs and anti-PMs lies in manipulating the expansion coefficients  $\Xi$  of the incident field. After that, the expansion coefficients  $\Psi$  of the scattered field can be obtained using Eq. (7). Finally, the desired incident and scattered fields can be reconstructed by linearly superimposing the corresponding VSHs using these coefficients. In Fig. 2(c-f), the scattered distributions of the particle under PM and anti-PM as incident fields in different refractive index environments can be observed more intuitively. Since our method can only describe the scattering field outside a sphere surrounding the particle of a specified radius<sup>25</sup>, a blank circle appears in the center of the images. Specific details and discussions are presented in the supplementary materials. The result verifies design method of the PMs, achieving a sensitivity to the environmental refractive index changes in the scattering of axisymmetric Mie particles.

### Method of generating PMs and anti-PMs

PMs and anti-PMs obtained above are both expressed as the combination of VSHs. Meanwhile, the tightly focused light field<sup>26</sup> can also be expanded by VSHs. In this work, we consider to generate PMs and anti-PMs by tightly focusing the paraxial beam by high-NA optical system. In order to achieve this goal, it is necessary to shape the wavefront of the paraxial beam on the pupil plane of the optical system to apply the desired field of PMs and anti-PMs on the Mie particle at the focusing point. In this work, we propose a convenient method to inversely design the paraxial beam by determining the relationship between paraxial beam and focusing field. Considering the complexity of PMs and anti-PMs, the distributions of amplitude, phase and polarization of the paraxial beam should be manipulated at the same time. Therefore, we represent the paraxial beam by radially polarized and azimuthally polarized components<sup>20</sup>, which is expressed as follows:

$$\mathbf{E}_p(r, \phi) = \sum_{\beta=1}^{\beta_{\max}} \sum_{m=-\beta}^{\beta} L_{\alpha\beta}(r) e^{i\alpha\phi} [u_{\alpha\beta} \mathbf{n}_r + v_{\alpha\beta} \mathbf{n}_\phi], \quad (12)$$

where  $\mathbf{n}_r$  and  $\mathbf{n}_\phi$  are the unit vectors along radial and azimuthal directions. Therefore, the paraxial beam consists of two kinds of vector modes.  $(\alpha, \beta)$  represent the mode orders of each vector mode.  $L_{\alpha\beta}(r)$  is a function that includes Laguerre polynomials<sup>27</sup>,  $u_{\alpha\beta}$  and  $v_{\alpha\beta}$  are the expansion coefficients for the radially polarized and azimuthally polarized components, respectively. When the theoretical model is considering for the particles with axially symmetry, the azimuthal order of light field should be conserved. The designed light fields of PMs and anti-PMs are both characterized by the specific azimuthal order with  $\mu=1$ . Therefore, only the terms in Eq. (12) with  $\alpha=1$  need to be included in the design of paraxial beam. Therefore, the expansion in Eq. (12) can be simplified as:

$$\mathbf{E}_p(r, \phi) = \sum_{\beta=1}^{\beta_{\max}} L_{\beta}(r) e^{i\phi} [u_{\beta} \mathbf{n}_r + v_{\beta} \mathbf{n}_\phi] \quad (13)$$

After passing through the high-NA system, the propagating directions and power distributions are modified. The paraxial beam in cylindrical coordinates is converted into a tightly focused beam in spherical coordinates after it passes through the lens, where  $\mathbf{n}_r$  is transformed into unit vector  $\mathbf{n}_\theta$  along polar angle direction. Then, we can obtain the far field angular distribution of the focusing field after passing through the aberration-correction objective.

$$\mathbf{E}_{\infty}(\theta, \phi) = \sum_{\beta=1}^{\beta_{\max}} P_{\beta}(\theta) e^{i\phi} [u_{\beta} \mathbf{n}_{\theta} + v_{\beta} \mathbf{n}_{\phi}], \quad (14)$$

where  $P_{\beta}(\theta)$  is the apodization function<sup>28</sup>, representing the amplitude distribution of the light field, which can be calculated by  $L_{\beta}(r)$  in Eq. (13).

To solve for the paraxial beam, the expansion coefficients  $u_{\beta}$  and  $v_{\beta}$  in Eq. (13) should be determined. Considering that the coefficients  $a_{\nu}$  and  $b_{\nu}$  for the PMs and anti-PMs are already obtained, we need to establish a M-matrix to express the relationship between two sets of coefficients, which depends on the characteristics of the high-NA optical system. The relationship can be expressed in Eq. (15).

$$\begin{bmatrix} a_1 \\ b_1 \\ \vdots \\ a_{\nu} \\ b_{\nu} \\ \vdots \end{bmatrix} = \begin{bmatrix} M_{11}^{(11)} & M_{11}^{(12)} & \cdots & M_{1\beta}^{(11)} & M_{1\beta}^{(12)} & \cdots \\ M_{11}^{(21)} & M_{11}^{(22)} & \cdots & M_{1\beta}^{(21)} & M_{1\beta}^{(22)} & \cdots \\ \vdots & \vdots & \ddots & \vdots & \vdots & \ddots \\ M_{\nu 1}^{(11)} & M_{\nu 1}^{(12)} & \cdots & M_{\nu\beta}^{(11)} & M_{\nu\beta}^{(12)} & \cdots \\ M_{\nu 1}^{(21)} & M_{\nu 1}^{(22)} & \cdots & M_{\nu\beta}^{(21)} & M_{\nu\beta}^{(22)} & \cdots \\ \vdots & \vdots & \ddots & \vdots & \vdots & \ddots \end{bmatrix} \begin{bmatrix} u_1 \\ v_1 \\ \vdots \\ u_{\beta} \\ v_{\beta} \\ \vdots \end{bmatrix} \quad (15)$$

With the inverse of the M-matrix, we can then use the focal field coefficients  $a_{\nu}$  and  $b_{\nu}$ , which correspond to the PMs and anti-PMs, to compute expansion coefficients  $u_{\beta}$  and  $v_{\beta}$  of the paraxial beam on pupil plane. The process of solving the M-matrix is similar with that for T-matrix discussed above. The key point is to determine the output modes after focusing process for each term of input field in Eq. (13).

We separately calculate the focal field distribution generated by the radially polarized and azimuthally polarized components. According to the Richards-Wolf vector diffraction integral formula<sup>26</sup>, the electric field near the focus can be obtained by integrating over a spherical wavefront with a radius equal to the focal length<sup>29</sup>:

$$\mathbf{E}(\rho, \varphi, z) = \frac{ikf e^{-ikf}}{2\pi} \int_0^{\theta_{\max}} \int_0^{2\pi} \mathbf{E}_{\infty}(\theta, \phi) e^{ikz \cos \theta} e^{ik\rho \sin \theta \cos(\phi - \varphi)} \sin \theta d\phi d\theta, \quad (16)$$

where  $(\rho, \varphi, z)$  are the spatial coordinates near the focus.  $\theta_{\max}$  is the numerical aperture angle of the lens, and  $\mathbf{E}_{\infty}(\theta, \phi)$  has been provided in Eq. (14).

To further expand the tightly focusing field by VSHs field, the vector field should be expressed in spherical coordinates rather than cylindrical coordinates. Then, the focal field distribution can be expanded using Eq. (13). In this way, the coefficients  $a_{\nu}$  and  $b_{\nu}$  can be derived based on orthogonality relation between two VSH field, thereby M-matrix can be solved. The corresponding paraxial vector beams to generate PMs and anti-PMs can be obtained. The amplitude and phase distributions of the x- and y-polarized components of the paraxial beam are shown in Fig. 3(b)-(i). To validate the inverse design method, we directly calculated the focusing fields of the paraxial beams depicted in Fig. 3 using the Richards-Wolf vector diffraction integral formula. The resulting expansion coefficients for  $a_{\nu}$  and  $b_{\nu}$  were found to be in agreement with the results for both PM and anti-PM fields. In practical experiments, we can employ Spatial Light Modulator (SLM) to generate the engineered incident light field<sup>30</sup> as derived above. However, it is crucial to consider the aberrations in the optical components and the environmental noise in real-world experiments.

## Conclusion

Our research has discovered a new efficient and accurate method for solving the T-matrix of axisymmetric particles and, through high-degree dynamic control of the light field, designs light fields that are sensitive or insensitive to refractive index changes. This allows us to enhance or suppress the impact of changes in the refractive index of the medium on the scattering effects of the particles. Additionally, we have calculated and determined the transmission matrix of the tightly focused system, enabling us to find specific incident vector beams from known focal field obtained by vector spherical harmonic expansion through the inverse design. The introduction of PMs and anti-PMs in the field of particle scattering alters the traditional understanding in frequency-domain manipulation of these modes. The PMs can be used to reduce the influence of environmental refractive index or other factors on particle scattering effects. The anti-PMs can enhance sensitivity in sensing applications. Moreover, the new solutions for the T-matrix of axisymmetric particles and the inverse design through the tightly focused system provide new insights and greater degrees of freedom for basic optical research and experimentation.

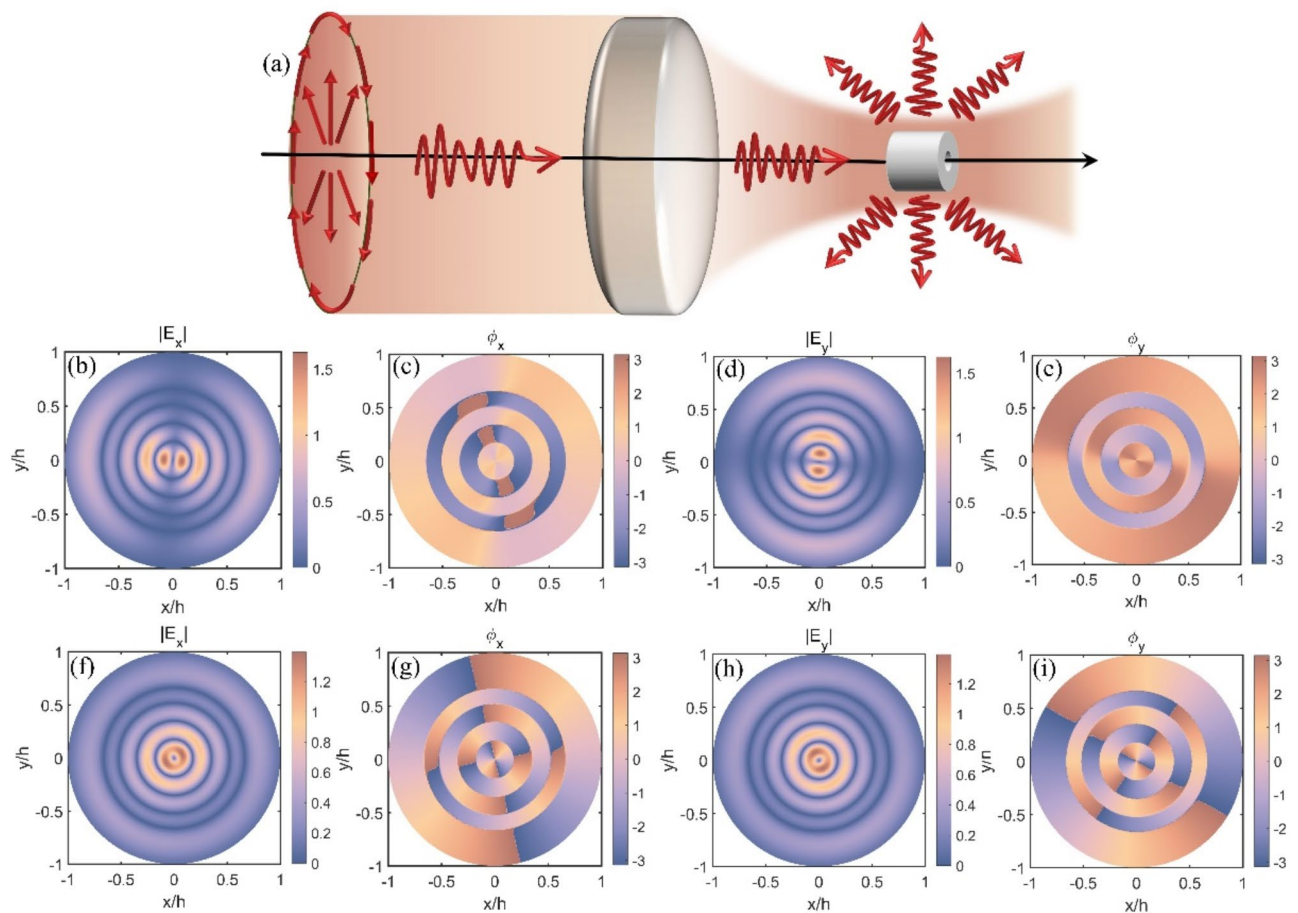


**Fig. 3.** (a) Schematic diagram of the tightly focused system. (b–e) Amplitude and phase distributions of the x and y components of the paraxial beam corresponding to the PMs. (f–i) Amplitude and phase distributions of the x and y components of the paraxial beam corresponding to the anti-PMs.  $h = f \sin \theta_{max}$  is the radius of the entrance pupil of the high-NA optical system<sup>26</sup>.

## Data availability

The datasets used and/or analysed during the current study available from the corresponding author on reasonable request.

Received: 27 December 2024; Accepted: 25 March 2025

Published online: 04 April 2025

## References

- Waterman, C. P. Matrix formulation of electromagnetic scattering. *Proc. IEEE*. **53**, 805–812 (1965).
- Mishchenko, M. I. & Travis, L. D. Capabilities and limitations of a current FORTRAN implementation of the T-matrix method for randomly oriented, rotationally symmetric scatterers. *J. Quant. Spectrosc. Radiative Transf.* **60**, 309–324 (1998).
- Poudel, S. *T-matrix Study of Scattering and Absorption of Light by Biomass Burning Aerosols* (North Carolina Agricultural and Technical State University, 2017).
- Gouesbet, G. & Gréhan, G. *Generalized lorenz-mie Theories* vol. 31 (Springer, 2011).
- Zhelyeznyakov, M. V., Zhan, A. & Majumdar, A. Design and optimization of ellipsoid scatterer-based metasurfaces via the inverse T-matrix method. *OSA Continuum*. **3**, 89–103 (2020).
- Miroshnichenko, A. E. et al. Nonradiating anapole modes in dielectric nanoparticles. *Nat. Commun.* **6**, 8069 (2015).
- Wei, L., Xi, Z., Bhattacharya, N. & Urbach, H. P. Excitation of the radiationless anapole mode. *Optica* **3**, 799–802 (2016).
- Hu, H., Gan, Q. & Zhan, Q. Achieving maximum scattering circular dichroism through the excitation of anapole States within chiral Mie nanospheres. *Phys. Rev. B*. **105**, 245412 (2022).
- Hell, S. W. et al. The 2015 super-resolution microscopy roadmap. *J. Phys. D Appl. Phys.* **48**, 443001 (2017).
- Otte, E. & Denz, C. Optical trapping gets structure: structured light for advanced optical manipulation. *Appl. Phys. Rev.* **7** (2020).
- Lee, B., Roh, S. & Park, J. Current status of micro- and nano-structured optical fiber sensors. *Opt. Fiber. Technol.* **15**, 209–221 (2009).
- Wang, L. V. & Hu, S. Photoacoustic tomography: in vivo imaging from organelles to organs. *Science* **335**, 1458–1462 (2012).
- Berchera, I. R. & Degiovanni, I. P. Quantum imaging with sub-Poissonian light: challenges and perspectives in optical metrology. *Metrologia* **56**, 024001 (2019).
- Piliarik, M., Kvasnička, P., Galler, N., Krenn, J. R. & Homola, J. Local refractive index sensitivity of plasmonic nanoparticles. *Opt. Express*. **19**, 9213–9220 (2011).



15. Ambichl, P. et al. Super- and anti-principal-modes in multimode waveguides. *Phys. Rev. X* **7**, 041053. <https://doi.org/10.1103/PhysRevX.7.041053> (2017).
16. Xiong, W. et al. Spatiotemporal control of light transmission through a multimode fiber with strong mode coupling. *Phys. Rev. Lett.* **117**, 053901 (2016).
17. Fyodorov, Y. V., Savin, D. V. & Sommers, H. J. Scattering, reflection and impedance of waves in chaotic and disordered systems with absorption. *J. Phys. Gen. Phys.* **38** (2005).
18. Rotter, S. & Gigan, S. Light fields in complex media: Mesoscopic scattering meets wave control.
19. Hell, S. W. Far-field optical nanoscopy. *Science* **316**, 1153–1158 (2013).
20. Novotny, L. & Hecht, B. *Principles of Nano-optics* (Cambridge University Press, 2012).
21. Pawley, J. B. *Handbook of Biological Confocal Microscopy* (Handbook of Biological Confocal Microscopy, 1990).
22. Ashkin, A., Dziedzic, J. M. & Yamane, T. Optical trapping and manipulation of single cells using infrared laser beams. *Nature* **330**, 769–771 (1987).
23. Zaman, M. A., Padhy, P. & Hesselink, L. Near-field optical trapping in a non-conservative force field. *Sci. Rep.* **9**, 649 (2019).
24. Bauer, T., Orlov, S., Peschel, U., Banzer, P. & Leuchs, G. Nanointerferometric amplitude and phase reconstruction of tightly focused vector beams. *Nat. Photonics* **8**, 23–27 (2014).
25. Bohren, C. F. & Huffman, D. R. *Absorption and Scattering of Light by Small Particles* (Wiley, 2008).
26. Richards, B. & Wolf, E. Electromagnetic diffraction in optical systems, II. Structure of the image field in an aplanatic system. *Proc. Royal Soc. Lond. Ser. Math. Phys. Sci.* **253**, 358–379 (1959).
27. Yang, Y., Li, Y. & Wang, C. Generation and expansion of Laguerre–Gaussian beams. *J. Opt.* **51**, 910–926 (2022).
28. Goodman, J. W. *Introduction To Fourier Optics* (Roberts and Company, 2005).
29. Born, M. & Wolf, E. *Principles of Optics: Electromagnetic Theory of Propagation, Interference and Diffraction of Light*. (Elsevier, 2013).
30. Han, W., Yang, Y., Cheng, W. & Zhan, Q. Vectorial optical field generator for the creation of arbitrarily complex fields. *Opt. Express* **21**, 20692–20706 (2013).

## Acknowledgements

This research was funded by the National Natural Science Foundation of China (62075132) and the Natural Science Foundation of Shanghai (22ZR1443100).

## Author contributions

J.Z. conceived the theoretical method(s), J.Z. and H.C. conducted the numerical simulation(s), J.L. and H.H. analysed the results. All authors reviewed the manuscript.

## Declarations

## Competing interests

The authors declare no competing interests.

## Additional information

**Supplementary Information** The online version contains supplementary material available at <https://doi.org/10.1038/s41598-025-95949-0>.

**Correspondence** and requests for materials should be addressed to H.H.

**Reprints and permissions information** is available at [www.nature.com/reprints](http://www.nature.com/reprints).

**Publisher's note** Springer Nature remains neutral with regard to jurisdictional claims in published maps and institutional affiliations.

**Open Access** This article is licensed under a Creative Commons Attribution-NonCommercial-NoDerivatives 4.0 International License, which permits any non-commercial use, sharing, distribution and reproduction in any medium or format, as long as you give appropriate credit to the original author(s) and the source, provide a link to the Creative Commons licence, and indicate if you modified the licensed material. You do not have permission under this licence to share adapted material derived from this article or parts of it. The images or other third party material in this article are included in the article's Creative Commons licence, unless indicated otherwise in a credit line to the material. If material is not included in the article's Creative Commons licence and your intended use is not permitted by statutory regulation or exceeds the permitted use, you will need to obtain permission directly from the copyright holder. To view a copy of this licence, visit <http://creativecommons.org/licenses/by-nc-nd/4.0/>.

© The Author(s) 2025